19th Australasian Fluid Mechanics Conference
Melbourne, Australia
8-11 December 2014

Turbulent Kinetic Energy and Temperature Variance Budgets in the Far Wake Generated by a Circular Cylinder

N. Lefeuvre[1], L. Djenidi[1], R. A. Antonia[1], T. Zhou[2]

[1]School of Engineering The University of Newcastle, NSW 2308, Australia
[2]School of Civil and Resource Engineering, The University of Western Australia, WA 6009, Australia

Abstract

Measurements of velocity and the temperature fluctuations have been performed to determine the budget of $\overline{q^2}$ (mean turbulence kinetic energy) and $\overline{\theta^2}$ (temperature variance) in the far wake of a cylinder. The two budgets show similar physical phenomena (advection and diffusion) as the source of large scale inhomogeneity on the flow centreline. It was noted that the estimates of the dissipation rates $\overline{\varepsilon}$ and $\overline{\chi}$ of $\overline{q^2}$ and $\overline{\theta^2}$, respectively, obtained using a spectral chart method results in a better closure in both the $\overline{q^2}$ and $\overline{\theta^2}$ budgets than their isotropic counterparts.

Introduction

The transport equations for both the turbulent kinetic energy, $\overline{q^2}$ [13] ($\equiv \overline{u^2}+\overline{v^2}+\overline{w^2}$), and the temperature variance, $\overline{\theta^2}$ [10], in plane wake can be approximated to

$$\frac{1}{2}U_1\frac{\partial \overline{q^2}}{\partial x}+\overline{uv}\frac{\partial \overline{U}}{\partial y}+\frac{\partial}{\partial y}\left(\frac{1}{2}\overline{vq^2}+\overline{p}\right) = -\overline{\varepsilon} \qquad (1)$$

$$\frac{1}{2}U_1\frac{\partial \overline{\theta^2}}{\partial x}+\overline{v\theta}\frac{\partial \overline{T}}{\partial y}+\frac{\partial}{\partial y}\left(\frac{1}{2}\overline{v\theta^2}\right) = -\overline{\chi}. \qquad (2)$$

$\overline{U}\equiv U_1-U_o$ and $\overline{T}$ are the mean velocity and temperature, U_1 and U_o are the free-stream velocity and the mean velocity deflect, u and v are the velocity fluctuations in the streamwise (x) and the lateral (y) direction and θ and p are the temperature and pressure fluctuations; $\overline{\varepsilon}$ is the mean turbulent kinetic energy dissipation rate and $\overline{\chi}$ is the mean temperature variance dissipation rate and are defined as

$$\overline{\varepsilon}=\frac{1}{2}\nu\overline{\left(\frac{\partial u_i}{\partial x_j}+\frac{\partial u_j}{\partial x_i}\right)^2} \qquad (3)$$

$$\overline{\chi}=\alpha\overline{\left(\frac{\partial \theta}{\partial x_i}\right)^2}, \qquad (4)$$

where ν and α are the kinematic viscosity and the thermal diffusivity, respectively.

There have been several attempts to measure the various terms in Eq. 1. In the far wake, Fabrice [8] and Browne et al. [4] have shown that the budget of q^2 on the centreline consists of a gain of energy, from the contributions of advection and turbulent diffusion, and a loss of energy due to $\overline{\varepsilon}$. As the distance from the axis increases, the production arises and balances the dissipation. It was also noted that the pressure diffusion term is small compared with the turbulent diffusion of $\overline{q^2}$. Browne et al. [4] and Browne and Antonia [1] highlight a strong anisotropy of both the $\overline{\varepsilon}$ and $\overline{\chi}$. The evaluation of ratios of velocity derivatives [4] and ratios of temperature derivatives [1] have shown a large departure from isotropic values. This fact appears to be a universal feature of shear flows and independent of the Reynolds number. Recently, Thiesset et al. [12] observed that the $\overline{q^2}$-budget in intermediate wake differs from that given in [4], where $\overline{\varepsilon}$ is balanced by advection only. This difference could be related to a reorganization or rescaling of the large-scale structures as they move from the intermediate wake field to the far wake field [3].

The closure of Eqs. 1 and 2 is a first step towards investigating the transport equations of $\overline{(\delta q)^2}$ ($\equiv \overline{\delta u^2}+\overline{\delta v^2}+\overline{\delta w^2}$) and $\overline{(\delta\theta^2)}$, where $\delta\alpha=\alpha(x+r)-\alpha(x)$, r is the spatial separation along x and $\alpha=u,\ v,\ w$ and θ. An interpretation of the transport equations of $\overline{(\delta q)^2}$ and $\overline{(\delta\theta^2)}$ is that they represent the energy and temperature budgets at each scale, which recover Eqs. 1 and 2, respectively, for very large separations r. There have been several attempts at investigating scale-by-scale (sbs) budgets, either experimentally or numerically, in various flows (e.g. homogeneous shear flow, centreline of a channel flow [6], circular jet [5] and intermediate wake flows [12]). In general, the closure of the budgets was relatively well validated, supporting the various assumptions made for deriving the equations. In these previously cited flows, different physical phenomena are at play. For example, grid turbulence and intermediate wake are dominated by the advection of energy, while the major source of inhomogeneity on the centreline of an axisymmetric jet is associated with the streamwise decay of turbulent energy with only a small contribution from the production.

In the present investigation, the budgets of $\overline{q^2}$ and $\overline{\theta^2}$ are measured in the far wake field of a two-dimensional circular cylinder turbulent wake, with special attention paid to the measurements of $\overline{\varepsilon}$ and $\overline{\chi}$. Experimental details are given in Sec. *II*. The one-point budgets for $\overline{\varepsilon}$ and $\overline{\chi}$ are obtained in Sec *III*. Sec. *IV* examines the effect of the shear on the second and third order structure functions of velocity and temperature. Finally, conclusions are drawn in Sec. *V*.

Experimental Apparatus

Measurements are carried out in an open circuit wind tunnel with a $2.4m$ long test section ($0.35m\times 0.35m$). The top wall of the working section is adjusted to achieve a zero mean pressure gradient. A circular cylinder of diameter $D=6mm$ is placed horizontally, spanning the whole test section. The measurements are carried out across the wake at a location of about $240D$ downstream of the cylinder. The upstream velocity was $U_1=3.6ms^{-1}$ corresponding to a Reynolds number based on the cylinder diameter of 1600 and a Taylor microscale Reynolds number $R_\lambda=44$ at the centerline of the wake.

The probe, sketched is in Fig. 1, consists of six wires, four operating at constant-temperature and two operating at constant current mode for measuring u at two spatial locations. The four hot wires, one X-wire and parallel hot wires, are arranged in order to measure one vorticity component. When the cross wire is in the (x,y) plane, u, v, and ω_z are obtained. Rotation through 90^o yields u, w and ω_y; ω_y and ω_z are the vorticity fluctuations in the y and z directions, respectively. The two wires, represented by h_1 and h_2 in Fig. 1 and which form the X-wire, are separated by $\Delta z=1.5mm$. the two hot parallel wires (h_3 and h_4 in Fig. 1) are separated by $\Delta y=1.5mm$. The separation of

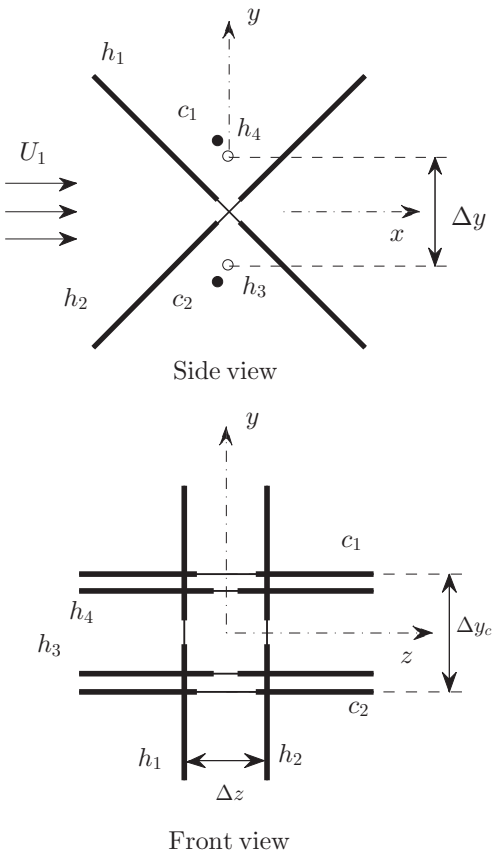

Figure 1: Schematic arrangement of probe.

parallel cold wires c_1 and c_2 is about $\Delta y_c = 2mm$. The spatial resolution of this probe was discussed in Zhou & Antonia [14]

All wires are etched from Wollaston $Pt-10\%Rh$ to an active length of about $200d_w$ for the hot wires ($d_w = 2.5\mu m$) and $1000d_w$ for the cold wires ($d_w = 0.63\mu m$). The output signals from the constant temperature and constant current circuits are digitized $12-bit$ analog-to-digital converter at a sampling frequency close to $2f_K = 1600$, where $f_K = U/2\pi\eta$ is the Kolmogorov frequency, after the low-pass filter cutoff frequency was set to be approximately equal to f_K. Each data acquisition lasts about $50s$. The time series of α ($\equiv u, v, w, \theta$) are used to construct temporal increments $\delta\alpha = \alpha(t+dt) - \alpha(t)$ required for two-point statistics. The Taylor hypothesis is then invoked to convert the temporal two-point signal $\delta\alpha$ into a two-point spatial signal.

Single Point Budgets of $\overline{q^2}$ and $\overline{\theta^2}$

Fig 2 and 3 show the distributions of $\overline{vu_i^2}$ and $\overline{v\theta}$ across half-width wake, respectively. Since only one component of $\overline{vq^2}$ was measured, the distribution of $\overline{vw^2}$ is inferred from our $\overline{vu^2}$ measurement and the anisotropy ratio $\overline{vw^2}/\overline{vu^2}$ measured by Fabrice [8]. Fig 2 shows a fairly general good agreement between the present distributions of $\overline{vu^2}$, $\overline{v^3}$ and $\overline{vw^2}$ and those of Browne [4]. The smaller amplitude of $\overline{vw^2}$ relatively to the other terms underlined a stronger lateral transport of $\overline{u^2}$ and $\overline{v^2}$ than for $\overline{w^2}$ [9]. The present distribution of $\overline{v\theta}$ collapses well on those of both [4] and [8]. Not shown here, the data of [4, 1] at $x/D = 420$ also show good collapse with the present measurements, suggesting that self-preservation is reached at the present streamwise location of measurements. This can then be exploited to estimate the gradient $\partial\overline{q^2}/\partial x$ (Eq. 1) and $\partial\overline{\theta^2}/\partial x$ (Eq. 2) using the streamwise variation of l_o, U_o and T_o. Under self-preservation, the following relations hold

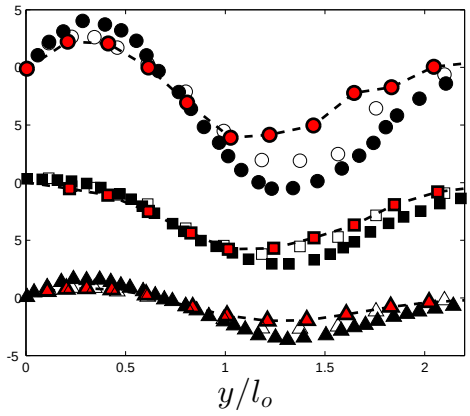

Figure 2: Distributions across the wake half-width of the triple velocity products that appear in the diffusion of energy due to lateral velocity fluctuations. ○, $\overline{vu^2}$; □, $\overline{v^3}$; △, $\overline{vw^2}$. (Open symbols: present data ; black symbols: Browne and al [4] ; red symbols with dashed line: Fabrice [8]). Note that a upward shift is applied to help visibility.

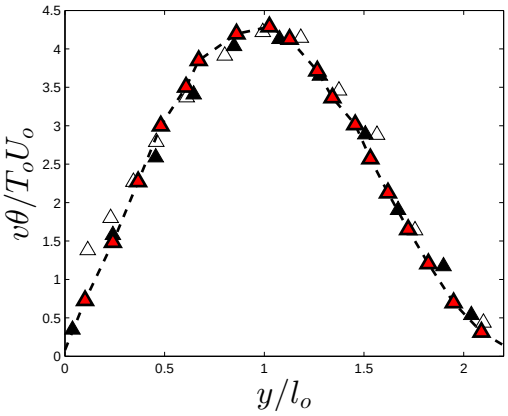

Figure 3: Distributions of lateral heat flux $\overline{v\theta}$ across the wake half-width. (Open symbols: present data ; black symbols: Browne and al [4] ; red symbols with dashed line: Fabrice [8])

$$\frac{l_o}{D} = 0.23\left(\frac{x-x_0}{d}\right)^{1/2} \tag{5}$$

$$\frac{U_o}{U_1} = 1.3\left(\frac{x-x_0}{d}\right)^{-1/2} \tag{6}$$

$$\frac{T_o}{T_1} = 25\left(\frac{x-x_0}{d}\right)^{-1/2}, \tag{7}$$

where l_o is the wake half width, U_o and T_0 are the maximum velocity deflect and mean temperature, T_1 and U_1 are the ambiance temperature and the free-stream velocity. The virtual origin x_0 is estimated to be -112. The data for q^2/U_o^2 and θ^2/T_o^2 are fitted with curves based on a cubic spline least-squares and numerical differentiation is applied on thess fits yielding $dh_q(\eta)/d\eta$ [11] and $dh_\theta(y/l_o)/d\eta$ ($\eta = y/l_o$), respectively. $U_o^2 h_q$ and $T_o^2 h_\theta$ are self-similar forms for $\overline{q^2}$ and $\overline{\theta^2}$. The lateral derivation of $\overline{U}$, $\overline{T}$, $\overline{v\theta^2}$ and $\overline{vq^2}$ are obtained in a similar manner.

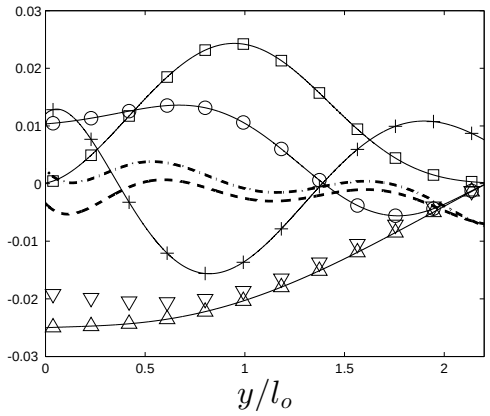

Figure 4: Measured budget of $\overline{q^2}$. ∘, advection; □, production; +, $\overline{q^2}$ diffusion; ▽, $\overline{\varepsilon}_{iso}$, △, $\overline{\varepsilon}$ from the spectral chart method and - - -, pressure diffusion (by difference using $\overline{\varepsilon}_{iso}$) ; - · -, pressure diffusion (by difference using $\overline{\varepsilon}$ from the spectral chart method). The maximum velocity defect, U_o, and the half-width wake, l_o, are used for the normalisation.

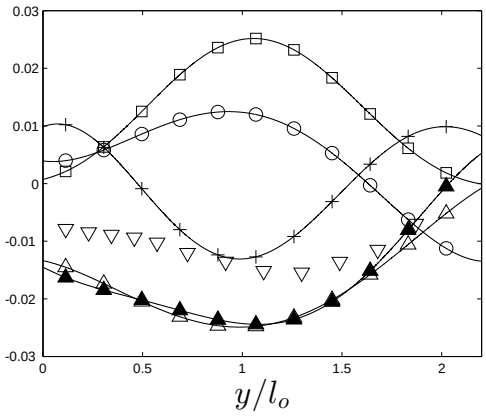

Figure 5: Measured budget of $\overline{\theta^2}$. ∘, advection; □, production; +, θ^2 diffusion; ▽, isotropic dissipation; ▲, full dissipation and △, optimum dissipation. The maximum velocity defect, U_o, and the half-width wake, l_o, are used for the normalisation.

Fig. 4 and 5 show all terms of Eq. 1 and 2 normalized by l_o/U_o^3. The term $\overline{\varepsilon}$ is estimated using two methods: the first one consists of assuming isotropy *i.e.* $\overline{\varepsilon} = \overline{\varepsilon}_{iso} = 15\nu\overline{(\partial u/\partial x)^2}$, the second uses a spectral chart method [7]. The rate $\overline{\chi}$ is calculated using both the isotropic relation ($\overline{\chi}_{iso} = 3\nu\overline{(\partial\theta/\partial x)^2}$ and Eq. 4. The pressure diffusion term obtained from $\overline{\varepsilon}_{iso}$ is small compared to the turbulent diffusion of q^2, and does not satisfy the integral constraint since its integration over the wake width is not 0. On the other hand, the pressure diffusion term obtained using estimate $\overline{\varepsilon}$ from the spectral chart method is consistent with the integral constraint. Similar to $\overline{\varepsilon}_{iso}$, the use of $\overline{\chi}_{iso}$ do not yield consistent results since it fails to produce a closed budget of θ^2. Note that the error between $\overline{\varepsilon}$ and $\overline{\varepsilon}_{iso}$ is about 20% on the centerline, while it is nearly 80% between $\overline{\chi}$ and $\overline{\chi}_{iso}$. The temperature dissipation appears to be more anisotropy than the kinetic energy dissipation.

Although not shown here, the budgets presented in [4] and [1], are in a qualitatively good agreement with those presented in Figures Fig. 4 and 5. The turbulent diffusion diffusion of q^2 is quantitatively similar to the turbulent diffusion of $\overline{\theta^2}$ across the wake. Near the wake axis, the transport of $\overline{q^2}$ through the mean velocity is nearly twice the transport of $\overline{\theta^2}$.

Two Point Statistics

We now look at two-point statistics as a first step toward a scale by scale analysis of the energy transfer between scales. The second- and third-order structure functions of q^2 and θ^2 may be written as

$$f_q = \frac{\overline{(\delta q)^2}}{\overline{q^2}} \qquad \textit{and} \qquad g_q = -\overline{(\delta u)(\delta q)^2}\frac{3^{1/2}R_\lambda}{\overline{q^2}^{3/2}} \tag{8}$$

$$f_\theta = \frac{\overline{(\delta\theta)^2}}{\overline{\theta^2}} \qquad \textit{and} \qquad g_\theta = -\overline{(\delta u)(\delta\theta)^2}\frac{3^{1/2}Pe}{(\overline{u^2}^{1/2}\overline{\theta^2})}. \tag{9}$$

f_q, f_θ, g_q and g_θ measured on the centerline ($y/l_o = 0$), and shown in Figures Fig. 4 and 5, indicate that the dissipation rates $\overline{\varepsilon}$ or $\overline{\chi}$ are balanced by advection and turbulent diffusion. At the locations $y/l_o = 0.25$ and $y/l_o = 1$, production and the diffusion term are maximum and minimum, respectively. Measured distributions of f_q and f_θ are shown Figs. 6(a) and 6(b) function of r/λ_q and r/λ_θ, respectively. There is a fairly good collapse of

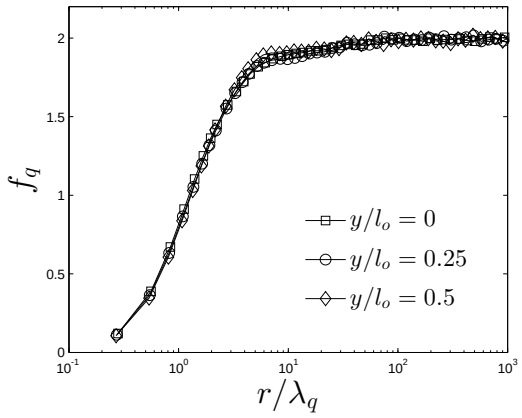

(a)

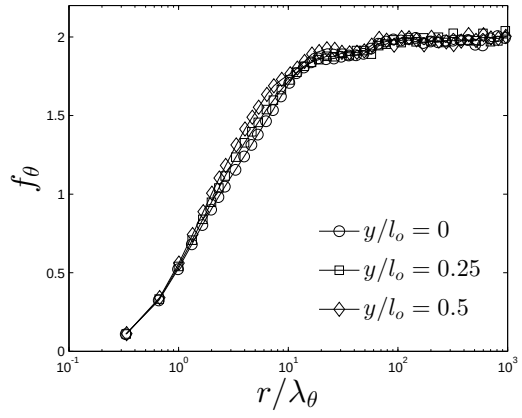

(b)

Figure 6: (a) f_q ($\equiv \overline{(\delta q)^2}/\overline{q^2}$) versus r/λ_q and (b) f_θ ($\equiv \overline{\delta\theta^2}/\overline{\theta^2}$) versus r/λ_θ across the wake.

f_q over practically the entire the scale separation range. The distributions of f_θ on the other hand present a weaker collapse, in particular in the range $2 \leq r/\lambda_\theta \leq 10$. Notice too, the overshoot in f_θ at $r/\lambda_\theta = 20$, while the asymptotic value of 2 for f_q is approached monotonically. The overshoot implies the temperature is more sensible to the presence of large-scale organisation that the velocity or kinetic energy. The differences between f_q

and f_θ have been already observed in different turbulence flows. For example, Antonia et al. have shown that f_q and f_θ differ in grid generated turbulence [2].

While one may consider that, overall, f_q and f_θ present good collapses across the wake, the third order structure functions do not show such features as seen in Fig. 7(a) and 7(b) which show g_q and g_θ function of r/λ_q and r/λ_θ, respectively. Both g_q and g_θ increase with y. Further analysis is being carried out to investigate the reason for this behaviour.

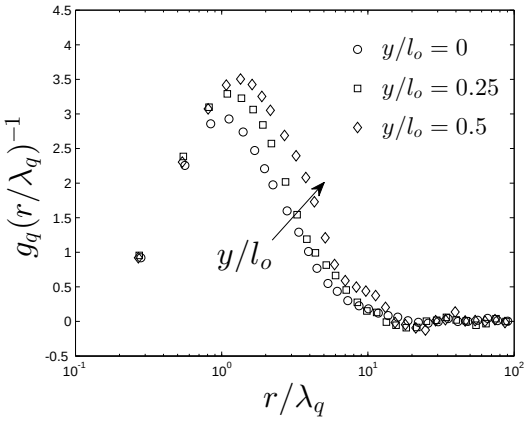

(a)

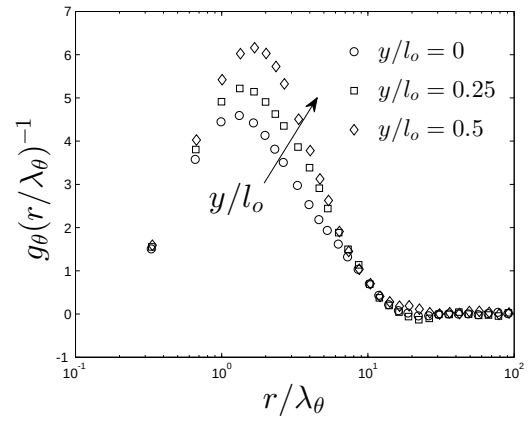

(b)

Figure 7: (a) g_q ($\equiv -\overline{\delta u(\delta q)^2}3^{1/2}R_{\lambda_q}/\overline{q^2}^{3/2}$) versus r/λ_q and (b) g_θ ($\equiv -\overline{\delta u(\delta\theta^2)}3^{1/2}R_{\lambda_q}/(\overline{u^2}^{1/3}\overline{\theta^2})$) versus r/λ_θ across the wake

Conclusions

Hot and cold wire measurements were carried out in a far field of a turbulent wake of a circular cylinder, with the aim to study the single-point budget of q^2 and θ^2. The measurements which were undertaken at the downstream streamwise location $x/D = 240$ showed that the first and second order statistics compared well with those of [4] and [1] at $x/D = 240$ and 420, suggesting that self-preservation is well approximated in the far field.

The results indicate that local isotropy is not satisfied. For example, it is found that using $\overline{\varepsilon}_{iso}$ and $\overline{\chi}_{iso}$ failed to provide closed budgets of q^2 and θ^2.

Two-points analysis showed that while the normalised second order structure functions f_q and f_θ evolve in self-similar manner across the wake, g_q and g_θ show variations across the wake.

References

[1] Antonia, R. and Browne, L., Anisotropy of the temperature dissipation in a turbulent wake, *Journal of Fluid Mechanics*, **163**, 1986, 393–403.

[2] Antonia, R. A., Smalley, R., Zhou, T., Anselmet, F. and Danaila, L., Similarity solution of temperature structure functions in decaying homogeneous isotropic turbulence, *Physical Review E*, **69**, 2004, 016305.

[3] Brown, G. L. and Roshko, A., Turbulent shear layers and wakes, *Journal of Turbulence*.

[4] Browne, L. W. B., Antonia, R. A. and Shah, D. A., Turbulent energy dissipation in a wake, *J . Fluid Mech.*, **1 79**, 1987, 307 – 326.

[5] Burattini, P., Antonia, R. A. and Danaila, L., Scale-by-scale energy budget on the axis of a turbulent round jet, *Journal of Turbulence*, **6**.

[6] Danaila, L., Anselmet, F., Zhou, T. and Antonia, R. A., Turbulent energy scale budget equations in a fully developed channel flow, *J. Fluid Mech.*, **430**, 2001, 87 – 109.

[7] Djenidi, L. and Antonia, R., A spectral chart method for estimating the mean turbulent kinetic energy dissipation rate, *Experiments in fluids*, **53**, 2012, 1005–1013.

[8] Fabris, G., *Conditionally sampled turbulent thermal and velocity fields in the wake of a warm cylinder and its interaction with an equal cool wake*, Ph.D. thesis, Illinois Institute of Technology, 1974.

[9] Fabris, G., Third-order conditional transport correlations in the two-dimensional turbulent wake, *Phys. Fluids*, **26**, 1983, 422 – 427.

[10] Freymuth, P. and Uberoi, M. S., Structure of temperature fluctuations in the turbulent wake behind a heated cylinder, *Physics of Fluids (1958-1988)*, **14**, 1971, 2574–2580.

[11] George, W. K., *The self-preservation of turbulent flows and its relation ti initial conditions and coherent structures*, Hemisphere NY, 1989.

[12] Thiesset, F., Antonia, R. and Danaila, L., Scale-by-scale turbulent energy budget in the intermediate wake of two-dimensional generators, *Physics of Fluids (1994-present)*, **25**, 2013, 115105.

[13] Townsend, A. A., The fully devoloped turbulence wake of a circuler cylinder, *Aust. J. Chem.*, **2**, 1949, 451.

[14] Zhou, T. and Antonia, R., Approximations for turbulent energy and temperature variance dissipation rates in grid turbulence, *Physics of Fluids*, **12**, 2000, 335–344.